SPACE-CHARGE-ENHANCED ENERGY MODULATION AT FERMI*

S. Khan†, Center for Synchrotron Radiation, TU Dortmund University, Dortmund, Germany
P. R. Ribič, C. Spezzani, S. Spampinati, E. Allaria, A. Brynes, G. Penco,
M. Trovò, L. Giannessi[2], G. De Ninno[3], Elettra-Sincrotrone Trieste SCpA, Basovizza, Italy
[1] also at Università degli Studi di Trieste, Trieste, Italy
[2] also at Laboratori Nazionali di Frascati, INFN, Frascati, Italy
[3] also at University of Nova Gorica, Nova Gorica, Slovenia

Abstract

High-gain harmonic generation (HGHG) is a seeding scheme for free-electron lasers (FELs), which improves the longitudinal coherence of the radiation output and reduces fluctuations of pulse energy, arrival time, and central wavelength compared to self-amplified spontaneous emission. In the HGHG scheme, a laser-induced energy modulation is followed by a dispersive section, where part of the electrons form density maxima ("microbunches") with the periodicity of the laser wavelength. The electrons between the microbunches have an energy spread correlated with the longitudinal coordinate. Longitudinal space charge (LSC) in a drift section tends to dilute the microbunches, while the correlated energy spread is flattened and can even change its sign. In this case, a second dispersive section can be used to form new density maxima from the electrons between the initial microbunches, and the resulting energy modulation amplitude may be significantly larger than the initial one. Results from experimental demonstrations of this novel LSC-enhanced modulation scheme at FERMI, a seeded FEL user facility in Trieste, Italy, are presented.

INTRODUCTION

The FERMI [1] user facility at the Elettra laboratory in Trieste, Italy, provides powerful radiation in the wavelength range from 100 to 4 nm with two free-electron laser (FEL) lines, FEL-1 [2] and FEL-2 [3]. Both rely on seeding schemes with an external laser, which improve the longitudinal coherence of the radiation output and reduce fluctuations of pulse energy, arrival time, and central wavelength compared to self-amplified spontaneous emission (SASE) [4]. In the high-gain harmonic generation (HGHG) scheme [5, 6], the interaction with a seed laser pulse in a short undulator ("modulator") leads to a sinusoidal modulation of the electron energy. In a subsequent dispersive section ("chicane"), part of the electrons form density maxima ("microbunches") with the periodicity of the laser wavelength, while the electrons between the microbunches have an energy spread correlated with the longitudinal coordinate as shown in Fig. 1(a). FEL amplification and coherent emission take place in a long undulator ("radiator") tuned to a harmonic of the seed wavelength. In order to extend the spectral range compared to the standard HGHG scheme, FEL-2 is based on two successive modulator-radiator stages [3], while FEL-1 was recently upgraded [7, 8] from HGHG to echo-enabled harmonic generation (EEHG) [9, 10], a seeding scheme involving two modulators and a radiator.

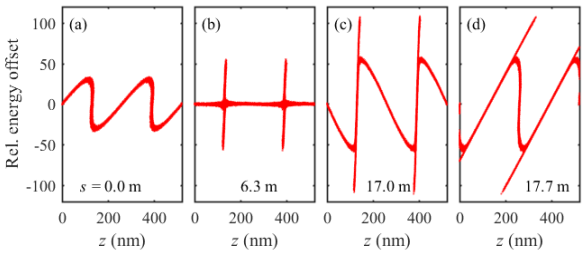

Figure 1: Distribution of electrons in longitudinal phase space, i.e., energy offset versus longitudinal position, (a) following a laser-induced energy modulation and a dispersive section, (b,c) after two different drift lengths s under the influence of LSC, and (d) after a second dispersive section.

Experimental investigations to study the effect of longitudinal space charge (LSC) on density-modulated electron bunches in drift sections were conducted at FEL-1 and FEL-2 [11–14]. LSC accelerates electrons ahead of each density maximum while trailing electrons are decelerated. This tends to broaden the microbunches and thus to reduce their bunching factor while the correlated energy spread between the microbunches is flattened as shown in Fig. 1(b), which may be advantageous for harmonic generation [15]. If the drift section is long enough, the correlated energy spread rises again with opposite sign opening the possibility to enhance an initially small laser-induced energy modulation as proposed in Ref. [13]. When the electron distribution of Fig. 1(c) passes another dispersive section, new microbunches are formed from the electrons between the initial density maxima as shown in Fig. 1(d). In the following, simulations and first experimental results of this LSC-enhanced modulation scheme are presented.

NUMERICAL SIMULATIONS

One-dimensional simulations are based on the coupled equations describing the motion of electrons in longitudinal phase space

$$\frac{dp_i}{d\tau} = \frac{2}{\alpha}\sum_{h=1}^{\infty} b_h \frac{\sin h\theta_i}{h} \quad \text{and} \quad \frac{d\theta_i}{d\tau} = \alpha\, p_i, \qquad (1)$$

* Work supported by Heinrich-Hertz-Stiftung, MKW NRW, and by the Bundesministerium für Forschung, Technologie und Raumfahrt (05K22PE1, 05K22PE4).
† shaukat.khan@tu-dortmund.de

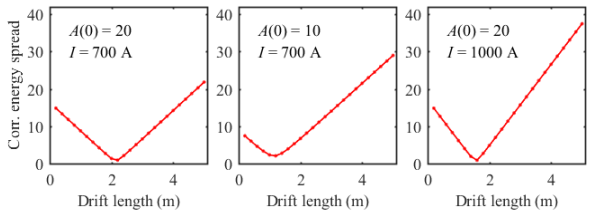

Figure 2: Amplitude of correlated energy spread for electrons between the microbunches as function of drift length for different combinations of initial modulation amplitude $A(0)$ and peak current I. For a given drift length, a higher final amplitude $A(s)$ is obtained by reducing $A(0)$ or increasing I.

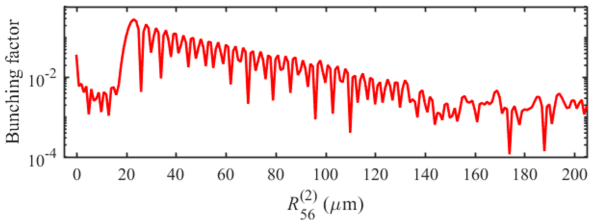

Figure 3: Example of the calculated bunching factor as function of the longitudinal dispersion $R_{56}^{(2)}$ of the second chicane with the first chicane optimized for HGHG.

here shown in the notation of Ref. [15]. The equations are iterated for macroparticles ($i = 1, \ldots n$) in small steps of plasma phase advance τ, which translates into position s in the laboratory frame via $\tau = k_\mathrm{P}\, s$, where

$$k_\mathrm{P} = \sqrt{\frac{e^2 n_0}{m_\mathrm{e} c^2 \varepsilon_0 \gamma_0^3}} \tag{2}$$

is the plasma wave number [16] with the electron charge $-e$ and mass m_e, the electron density n_0, the dielectric constant ε_0, and the Lorentz factor γ_0. The phase space coordinates are the relative energy offset $p_i = \eta_i/\sigma_\eta$ with $\eta_i \equiv (\gamma_i - \gamma_0)/\gamma_0$ normalized to the relative energy spread σ_η and the phase $\theta_i = k_\mathrm{L} z_i = 2\pi z_i/\lambda_\mathrm{L}$ with the laser wavelength λ_L and the longitudinal coordinate z_i in a co-moving frame. Furthermore,

$$b_h = \frac{1}{n}\left|\sum_{i=1}^{n} \exp(ih\theta_i)\right| \tag{3}$$

is the bunching factor at laser harmonic h, which is updated at every iteration, and the parameter $\alpha \equiv (k_\mathrm{L}/k_\mathrm{P})\,\sigma_\eta/\gamma_0^2$ normalizes the frequency of the plasma oscillation given by Eq. (1). The first of the coupled equations describes the energy change due to a longitudinal electric field caused by a gradient of the charge distribution. The second equation can be rewritten as $dz_i/ds = \eta_i/\gamma^2$ meaning that relativistic particles with an energy offset change their longitudinal position due to velocity mismatch.

In the example of Fig. 1, the final energy modulation amplitude exceeds the initial one by a factor of 2 and the calculated bunching factor is significantly enhanced. In good approximation, the energy modulation amplitude $A(s)$ normalized to the energy spread changes linearly with drift length s according to

$$A(s) = |g| \cdot s - A(0). \tag{4}$$

Here, $|g| = |dA/ds| = A(0)/s^*$ is the gradient of amplitude changing with s, and s^* is the drift length at which the correlated energy spread is flat. The gradient is given by the electron density (or peak current), but is largely independent of $A(0)$. As a counterintuitive result, the final modulation amplitude after a given drift length is larger when the initial one is smaller. In this case, s^* is shorter and leaves more of the remaining drift length for the modulation with opposite sign to develop. Figure 2 shows three examples with different initial modulation amplitude and peak current.

In order to verify the existence of a phase space distribution as in Fig. 1(d) experimentally, the longitudinal dispersion $R_{56}^{(1)}$ of the first chicane is tuned to maximize the HGHG signal and then the dispersion $R_{56}^{(2)}$ of the second chicane is scanned. The calculation in Fig. 3 shows that the bunching factor decreases when $R_{56}^{(2)}$ rises above zero and increases rapidly again when approaching the phase space distribution of Fig. 1(d) with one maximum of the electron density per seed wavelength. A further increase of $R_{56}^{(2)}$ leads to a double peak per wavelength and a succession of smaller maxima of the bunching factor. These maxima occur when the double peak separation matches an integer multiple of the FEL wavelength. While the calculation of Fig. 3 was performed for a constant modulation amplitude, the maxima of the bunching factor are expected to be smeared out in an experiment, where the amplitude varies along the seed pulse.

EXPERIMENTAL RESULTS

Measurements were performed at both FEL lines of FERMI. After being upgraded for EEHG [8], the new configuration of FEL-1 is

$$\mathrm{M1} \rightarrow \mathrm{DS1} \rightarrow \mathrm{M2} \rightarrow \mathrm{DS2} \rightarrow \mathrm{R}.$$

With two dispersive sections, FEL-1 is well-suited to test the LSC-enhanced seeding scheme. Here, the laser-electron interaction took place in the first modulator M1 while the second modulator M2 with fully open magnetic gap acted as a drift space. The two dispersive sections, DS1 and DS2, were employed as described above, and the radiator R consisted of six 2.4 m long undulator modules.

After tuning the longitudinal dispersion of DS1 for optimum HGHG signal, the longitudinal dispersion $R_{56}^{(2)}$ of DS2 was scanned in steps of 2 µm. The energy values of 50 FEL pulses per step were recorded using a monitor based on the photo-ionization of a low-density rare gas [17]. The measurements were performed for different seed pulse energies and peak currents. Figure 4 shows an example in which the scan was repeated with 1 to 6 undulator modules acting as radiator. This allows to extract a gain curve, i.e., pulse

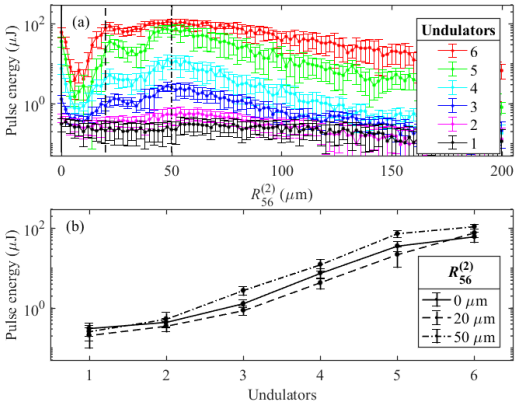

Figure 4: (a) Scan of the longitudinal dispersion $R_{56}^{(2)}$ of the second chicane in FEL-1 while recording the FEL pulse energy. The length of the radiator was varied by closing the magnetic gap of 1 to 6 undulator modules. (b) Gain curves for three values of $R_{56}^{(2)}$.

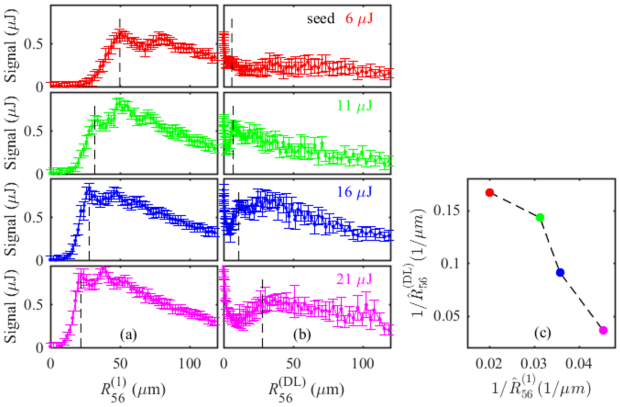

Figure 5: (a,b) Scans of the longitudinal dispersion $R_{56}^{(1)}$ of the first chicane and $R_{56}^{(DL)}$ of the delay line in FEL-2 while recording the FEL pulse energy for different seed pulse energies. Dashed lines mark the values $\hat{R}_{56}^{(1)}$ and $\hat{R}_{56}^{(DL)}$ of the respective first maximum. (c) The LSC-induced energy modulation amplitude $\sim 1/\hat{R}_{56}^{(DL)}$ increases for decreasing initial amplitude $\sim 1/\hat{R}_{56}^{(1)}$.

energy as function of radiator length, for each $R_{56}^{(2)}$ value. As expected, the signal decreases with nonzero $R_{56}^{(2)}$ and rises again due to the formation of new microbunches, followed by a tail of merging secondary peaks. The pulse energy around $R_{56}^{(2)} = 50\,\mu\text{m}$ is significantly (factor 1.7) higher than the HGHG signal at zero $R_{56}^{(2)}$.

Upon closer inspection, the measurement deviates in several aspects from the calculated bunching factor in Fig. 3. Since the modulation amplitude is lower on the slopes of the seed pulse, the HGHG signal has a tail towards higher $R_{56}^{(2)}$ while the LSC-induced peaks should have tails towards lower $R_{56}^{(2)}$, because a lower initial amplitude $A(0)$ leads to higher $A(s)$ of the new microbunches according to Eq. (4). The FEL signal after the radiator depends on the gain curve. Figure 4(b) shows saturation for the HGHG signal (solid curve) and $R_{56}^{(2)} = 50\,\mu\text{m}$ (dotted-dashed) but for 20 µm (dashed) the gain curve still rises. The occurrence of two maxima with a dip at $R_{56}^{(2)} = 30\,\mu\text{m}$ and similar observations in other measurements suggest that the electron distribution is not homogeneous. Variations in electron density lead to different gradients g and final amplitudes $A(s)$ in Eq. (4). The respective $R_{56}^{(2)}$ values scale with $1/A(s)$.

Another set of measurements was performed at the FEL-2 line, where the configuration

$$\text{M1} \rightarrow \text{DS1} \rightarrow \text{R1} \rightarrow \text{DL} \rightarrow \text{M2} \rightarrow \text{DS2} \rightarrow \text{R2}$$

was designed for two-stage HGHG seeding [3]. After laser-electron interaction in modulator M1, chicane DS1 and the delay line DL were employed for the LSC scheme while radiator R1 was disabled. The modulator M2 acted as radiator, since the undulators of R2 are designed for shorter wavelengths. Despite the short radiator, signals from the LSC-induced modulation were clearly detected – see Fig. 5. In the scans for different seed pulse energy, the respective energy modulation amplitude is proportional to the inverse longitudinal dispersion of the first maximum. According to Fig. 5 (c), the LSC-induced modulation amplitude increases with decreasing seed pulse energy, i.e., smaller laser-induced amplitude, as expected. For small initial modulation, the $\hat{R}_{56}^{(DL)}$ values suggest LSC-induced amplitudes exceeding the FEL bandwidth, which may be the reason for the small signal at seed pulse energy 6 µJ.

SUMMARY AND CONCLUSIONS

Coherent radiation emission after LSC-induced reversal of the correlated energy spread and formation of new microbunches in a second dispersive section has been demonstrated in both FEL lines of FERMI. Depending on seed pulse energy and peak current, the observed FEL pulse energies may exceed those of HGHG significantly and the results are consistent with numerical simulations in longitudinal phase space. Linear relations as in Eq. (4) are expected to be modified by three-dimensional effects. The signal is very sensitive to variations of the peak current and other electron and laser parameters [13]. The influence of an inhomogeneous electron distribution and variations of FEL gain along the radiator require further investigation. An enhancement of the energy modulation amplitude is particularly attractive when the initial amplitude is small, e.g., in seeded FELs with high repetition rate, or to recover from the debunching effect in an unavoidable drift section.

ACKNOWLEDGEMENTS

S. K. would like to acknowledge the kind hospitality of the FERMI team and the support during the measurements and data analysis.

REFERENCES

[1] E. Allaria *et al.*, "The FERMI free-electron lasers", *J. Synchrotron Radiat.*, vol. 22, pp. 485–491, 2015. doi:10.1107/S1600577515005366

[2] E. Allaria *et al.*, "Highly coherent and stable pulses from the FERMI seeded free-electron laser in the extreme ultraviolet", *Nat. Photonics*, vol. 6, pp. 699–704, 2012. doi:10.1038/nphoton.2012.233

[3] E. Allaria *et al.*, "Two-stage seeded soft-X-ray free-electron laser", *Nat. Photonics*, vol. 7, pp. 913–918, 2013. doi:10.1038/nphoton.2013.277

[4] A. M. Kondratenko and E. L. Saldin, "Generating coherent radiation by a relativistic electron beam in an ondulator," *Part. Accel.*, vol. 10, pp. 207–216, 1980.

[5] L. H. Yu, "Generation of intense uv radiation by subharmonically seeded single-pass free-electron lasers", *Phys. Rev. A*, vol. 44, pp. 5178-5193, 1991. doi:10.1103/PhysRevA.44.5178

[6] L.-H. Yu and I. Ben-Zvi, "High-gain harmonic generation of soft X-rays with the "fresh bunch" technique", *Nucl. Instrum. Methods Phys. Res. A*, vol. 393, pp. 96-99, 1997. doi:10.1016/S0168-9002(97)00435-X

[7] P. Rebernik Ribič *et al.*, "Coherent soft X-ray pulses from an echo-enabled harmonic generation free-electron laser", *Nat. Photonics*, vol. 13, pp. 555-561, 2019. doi:10.1038/s41566-019-0427-1

[8] C. Spezzani *et al.*, "Echo-enabled harmonic generation at FERMI FEL-1: Commissioning and initial user experience", in *Proc. 15th Int. Particle Accelerator Conf. (IPAC'24)*, Nashville, TN, USA, May 2024, pp. 1889–1892. doi:10.18429/JACoW-IPAC2024-WEAD3

[9] G. Stupakov, "Using the beam-echo effect for generation of short-wavelength radiation", *Phys. Rev. Lett.*, vol. 102, p. 074801, 2009. doi:10.1103/PhysRevLett.102.074801

[10] D. Xiang and G. Stupakov, "Echo-enabled harmonic generation free electron laser", *Phys. Rev. ST Accel. Beams*, vol. 12, p. 030702, 2009. doi:10.1103/PhysRevSTAB.12.030702

[11] S. Khan *et al.*, "Evolution of microbunching in drift sections", in *Proc. 40th Int. FEL Conf. (FEL'22)*,, Trieste, Italy, Aug. 2022, pp. 21–24. doi:10.18429/JACoW-FEL2022-MOP01

[12] S. Khan *et al.*, "Space charge effects of density-modulated electron beams in drift spaces", in *Proc. 14th Int. Particle Accelerator Conf. (IPAC'23)*, Venice, Italy, May 2023, pp. 1835–1838. doi:10.18429/JACoW-IPAC2023-TUPL033

[13] S. Khan *et al.*, "Evolution of density-modulated electron beams in drift sections", *Phys. Rev. Accel. Beams* vol. 27, p. 040702, 2024. doi:10.1103/PhysRevAccelBeams.27.040702

[14] S. Khan *et al.*, "Demonstration of space-charge-enhanced energy modulation at FERMI", in *Proc. SPIE 13536, X-Ray Free-Electron Lasers*, Prague, Czech Republic, Apr. 2025, p. 1353601. doi:10.1117/12.3075768

[15] E. Hemsing *et al.*, "Correlated Energy-Spread Removal with Space Charge for High-Harmonic Generation", *Phys. Rev. Lett.*, vol. 113, p. 134802, 2014. doi:10.1103/PhysRevLett.113.134802

[16] J. Rosenzweig, C. Pellegrini, L. Serafini, C. Ternieden, and G. Travish, "Space-charge oscillations in a self-modulated electron beam in multi-undulator free-electron lasers", *Nucl. Instrum. Methods Phys. Res. A*, vol. 393, pp. 376–379, 1997. doi:10.1016/S0168-9002(97)00516-0

[17] M. Zangrando *et al.*, "The photon analysis, delivery, and reduction system at the FERMI@Elettra free electron laser user facility", *Rev. Sci. Instrum.*, vol. 80, p. 113110, 2009. doi:10.1063/1.3262502